The Cryosphere Discuss., 9, 183–221, 2015
www.the-cryosphere-discuss.net/9/183/2015/
doi:10.5194/tcd-9-183-2015

The Cryosphere Discussions
Open Access

Modelling the impact of submarine frontal melting and ice mélange on glacier dynamics

J. Krug[1,2], **G. Durand**[1,2], **O. Gagliardini**[1,2,3], **and J. Weiss**[1,2]

[1]CNRS, LGGE, 38041 Grenoble, France
[2]Univ. Grenoble Alpes, LGGE, 38041 Grenoble, France
[3]Institut Universitaire de France, Paris, France

Received: 1 December 2014 – Accepted: 14 December 2014 – Published: 9 January 2015

Correspondence to: J. Krug (jean.krug@lgge.obs.ujf-grenoble.fr)

Published by Copernicus Publications on behalf of the European Geosciences Union.

Abstract

Two mechanisms are generally proposed to explain seasonal variations in the calving front of tidewater glaciers: submarine melting of the calving face and the mechanical back-force applied by the ice mélange. However, the way these processes affect the calving rate and the glacier dynamics remains uncertain. In this study, we used the finite element model Elmer/Ice to simulate the impact of these forcings on more than 200 two dimensional theoretical flowline glacier configurations. The model, which includes calving processes, suggests that frontal melting affects the position of the terminus only slightly (< a few hundred meters) and does not affect the pluriannual glacier mass balance at all. However, the ice mélange has a greater impact on the advance and retreat cycles of the glacier front (more than several 1000 m) and its consequences for the mass balance are not completely negligible, stressing the need for better characterization of forcing properties. We also show that ice mélange forcing against the calving face can mechanically prevent crevasse propagation at sea level and hence prevent calving. Results also revealed different behaviors in grounded and floating glaciers: in the case of a floating extension, the heaviest forcings can disrupt the glacier equilibrium by modifying its buttressing and ice flux at the grounding line.

1 Introduction

In the context of global warming, the cryosphere's contribution to sea level rise is a major concern. Depending on the four RCP scenarios (Representative Concentration Pathways for greenhouse gas concentration pathways) considered in the IPCC fifth assessment (Church et al., 2013), the sea level is predicted to rise between 0.26 and 0.82 m in 2081–2100, relative to 1986–2005. The Greenland Ice Sheet (GIS) negative mass balance, which was $-142 \pm 49\,\mathrm{Gt\,a^{-1}}$ on average over the past two decades, has increased in recent years, to reach an estimated value of $-263 \pm 30\,\mathrm{Gt\,a^{-1}}$ between 2005 and 2010 (Schrama and Wouters, 2011; Shepherd et al., 2012) and

TCD
9, 183–221, 2015

$-359.8 \pm 28.9\,\mathrm{Gt\,a^{-1}}$ from April 2009 to April 2012 (Khan et al., 2014). This mass loss extended over a large part of the GIS (Khan et al., 2010, 2014; Schrama and Wouters, 2011), which is thus becoming a major contributor to sea level rise (SLR) (Cazenave, 2006; Rignot et al., 2011).

Increasing ice loss highlights the need for accurate estimations of the future mass balance, but the large discrepancies in the behavior of Greenland's outlet glaciers make a simple mass balance extrapolation unreliable, unless we understand the processes that control their dynamics (Howat et al., 2011; Seale et al., 2011). The mass loss from the GIS is the consequence of two main mechanisms: the dynamic ice discharge (through calving and frontal melting) and the negative surface mass balance (SMB). Ice discharge was estimated to represent 40 to 60 % of the total mass loss (Rignot et al., 2008; van den Broeke et al., 2009; Khan et al., 2014), corresponding to $-156.3 \pm 40.9\,\mathrm{Gt\,a^{-1}}$. Ice discharge is therefore an unavoidable mechanism, and the two related processes (melting and calving) not only directly affect the position of the front, but also affect the force imbalance at the front: feedback between ice discharge and ice flow are therefore to be expected.

Holland et al. (2008) hypothesized that the increased discharge in Greenland may have been triggered by an increase in the subsurface ocean temperature. This claim was supported by Straneo et al. (2010), who stated that a rapid advective pathway exists between North Atlantic's oceanic variability and the margin of the ice shelf in the vicinity of Sermilik Fjord, East Greenland. The underlying process suggests that submarine frontal melting promotes the emergence of an ice bloc overhanging the water line, which calves rapidly due to an *undercutting effect*. Remote observations of east GIS glaciers revealed a correlation between variations in the position of the terminus and variations in the temperature of the ocean (Seale et al., 2011). However, melting intensity is hard to measure accurately and is usually inferred from hydrographic measurements (water velocity, temperature and salinity) of the heat transport within the water layers. Thus, summer melt rates vary between 1 and $17\,\mathrm{m\,day^{-1}}$, depending on

TCD
9, 183–221, 2015

the glacier and the associated fjord system (Motyka et al., 2003; Rignot et al., 2010; Sutherland and Straneo, 2012; Bartholomaus et al., 2013; Inall et al., 2014).

Another process, that of ice mélange, a heterogeneous mixture of sea ice, marine ice, blown snow, and fragments of icebergs, is suspected to play an important role in the seasonal cycles of the glacier front (Higgins, 1991; Sohn et al., 1998; Reeh et al., 2001; Khazendar and Jenkins, 2003; Fricker et al., 2005; Copland et al., 2007; Joughin et al., 2008a, b, c). Observations showed that winter freezing of the ice mélange is correlated with a decrease in the calving rate, an advance of the glacier front and a slowing down of the ice flow (Sohn et al., 1998; Joughin et al., 2008c), and that summer decay is followed by an increase in the calving rate, a retreat of the front and accelerated ice flow (Higgins, 1991; Copland et al., 2007). Some authors argue that ice mélange may directly resist the ice flow (Walter et al., 2012), while others suggest that it only maintains the integrity of the terminal part of the glacier (Sohn et al., 1998; Amundson et al., 2010). Thus, although variations in the position of the terminus and the existence of a layer of ice mélange layer are clearly correlated, the underlying processes that control this behavior are still poorly understood.

Several attempts have been made to incorporate frontal melting and the ice mélange back-force in ice flow models. In particular, the relation between calving and undercutting was investigated by Vieli et al. (2002), who applied a seasonal calving pattern on a simplified geometry of Hansbreen Glacier, in Svalbard, assuming that calving was controlled by melting at the water line. These authors concluded that melting-driven calving only had a minor impact on glacier dynamics. On the contrary, O'Leary and Christoffersen (2013) used fixed geometry to investigate the effect of different melting patterns on the stress field in the ice. These authors showed that undercutting can be a strong driver of calving, due to the concentration of stress that occurs at the upper surface. However, recent studies using calving parameterization based on an instantaneous stress balance (Benn et al., 2007a, b; Nick et al., 2009, 2010) applied on 2-D-simplified geometries of Helheim (Cook et al., 2014) and Store Glaciers (Todd and Christoffersen, 2014), tempered these conclusions. According to Cook et al. (2014),

TCD
9, 183–221, 2015

when undercut, the upper surface of the glacier drops, thereby reducing tensile stress. The effect of ice mélange on glacier dynamics was analyzed by Nick et al. (2010) and Vieli and Nick (2011) using a depth and width-integrated model combined with Nick et al. (2010)'s calving parameterization. Both studies managed to reproduce the cycles of advance and retreat of the glacier fronts with realistic amplitudes. However, the authors did not undertake further investigation of the underlying processes. Cook et al. (2014) stated that only unrealistically high back-pressure would be able to change the position of the front, highlighting the need for further modelling focused on processes, whereas Todd and Christoffersen (2014) applied a back-force similar to the one evaluated by Walter et al. (2012) to Store's calving front, and showed that this realistic forcing could have a significant impact on the advance and retreat cycles of the glacier front.

In this article, we examine the consequence of submarine frontal melting and the ice mélange on glacier dynamics and on the behavior of the glacier front using a full-Stokes ice-flow finite element model combined with calving parameterization based on damage and fracture mechanics. This enables a complete representation of the stress field in the vicinity of the front, and provides a reliable tool to study front dynamics. To be sure our conclusions are robust for a number of glacier geometries and flow specifications, we ran more than 200 simulations combining a wide range of glacier sizes, flow and damage parameters, and forcing constraints. We provide a brief description of the model in Sect. 2, and in Sect. 3, we describe the setup and list the parameters. In Sect. 4, we describe glacier responses to seasonally variable forcings, and in Sect. 5, we provide a deeper analysis of the processes and mechanisms and compare the behavior of grounded and floating glaciers.

TCD
9, 183–221, 2015

2 Model presentation

2.1 Ice-flow model

We considered an incompressible, isothermal, and gravity-driven ice flow. The ice exhibits non-linear viscosity, and the flow is ruled by the Stokes equations, which reads:

$$\mathrm{div}(\boldsymbol{\sigma}) + \rho_\mathrm{i}\boldsymbol{g} = 0 \quad (1)$$

$$\mathrm{div}(\boldsymbol{u}) = 0 \quad (2)$$

where $\boldsymbol{\sigma}$ represents the Cauchy stress tensor, $\boldsymbol{g}$ the gravity force vector, ρ_i the density of ice and $\boldsymbol{u}$ the velocity vector. The Cauchy stress tensor can be expressed as a function of the deviatoric stress tensor $\mathbf{S}$ and the cryostatic pressure p with $\boldsymbol{\sigma} = \mathbf{S} - p\mathbf{I}$ and $p = -\mathrm{tr}(\boldsymbol{\sigma})/3$. Ice rheology is represented by a non-linear Norton–Hoff type flow law called *Glen's flow* law, which can be expressed as:

$$\mathbf{S} = 2\eta\dot{\boldsymbol{\epsilon}} \quad (3)$$

This equation links the deviatoric stress tensor $\mathbf{S}$ to the strain rate tensor $\dot{\boldsymbol{\epsilon}}$. The effective viscosity η is written:

$$\eta = \frac{1}{2}(EA)^{-1/n} I_{\dot{\epsilon}_2}^{(1-n)/n} \quad (4)$$

where $I_{\dot{\epsilon}_2}^2$ represents the square of the second invariant of the strain rate tensor, A is the fluidity parameter and E is an *enhancement factor*. A complete description of the model can be found in Gagliardini et al. (2013).

2.2 Damage model

The ice-flow model described above was coupled with a calving model based on damage and fracture mechanics. Damage mechanics was used to describe the degradation

TCD
9, 183–221, 2015

of the mechanical properties of ice under the stress field, averaged at a mesoscale. Under sufficient stress, the ice is damaged and its viscosity is reduced. The level of isotropic damage in the ice is quantified by a scalar variable D called damage variable, which equals zero for virgin ice and tends to 1 for fully damaged ice. Crevasse fields at the surface of a glacier can then be represented, and a stress history of the ice recorded.

This damage model was coupled with a linear elastic fracture mechanics (LEFM) model, which was used to represent the rapid propagation of crevasses that characterizes calving events. In LEFM, the initiation of crevasse propagation depends on the stress intensity factor K_I. To trigger propagation, the stress intensity factor, which depends on the size of the initial flaw and on the stress field, must be higher than the ice toughness K_{Ic}. An initial crevasse depth provided by the previously computed damage field was used to compute the stress intensity factor. Once propagation is initiated, the stress intensity factor is computed at sea level. If the stress intensity factor is higher than an arrest criterion K_{Ia}, the crevasse continues to propagate until it reaches the bottom of the glacier, and triggers calving.

Among the numerical parameters required to run the model, three have to be calibrated, and are discussed below: the damage critical value D_c, a stress threshold σ_{th}, and a damage enhancement factor B. The criterion $D > D_c$ gives a shape to the depth of pre-existing flaws, σ_{th} is the load that has to be applied to trigger ice degradation, and B quantifies the rate at which damage increases.

The model summarized here is described in detail in Krug et al. (2014) and implemented in the finite element open-source model Elmer/Ice (see Gagliardini et al., 2013).

TCD
9, 183–221, 2015

3 Setup and forcing parameterization

3.1 Geometries and boundary conditions

We wanted to generalize our conclusions to a wide range of two-dimensional synthetic flowline glacier geometries, of time-varying length (L) and thickness (H). To this end, we built 60 geometries that depend on five parameters: the inlet ice flux (F_{inlet}), water depth (H_{w}), and damage parameters (σ_{th}, B, D_{c}). These parameters were sampled using a Latin Hypercube Sampling (LHS) method, and the glaciers were built up from ice slabs initially grounded on a linear analytical prograde slope (1 %). The meshes comprise $\sim$ 7000 quadrilateral elements. Horizontally, the refinement is higher at the front (10 to 15 m) and in the vicinity of the upper surface (2 to 3 m), to account for the processes that occur at the calving front, as well as the production of damage and advection at the upper surface. The setup is illustrated in Fig. 1.

Boundary conditions are the same as those given in Krug et al. (2014). In addition, some specific conditions are given below:

- At the bed, the glacier can be either grounded or floating. The grounding line position is obtained through the resolution of a contact problem (Durand et al., 2009).
- As glacier thickness can vary with time, instead of prescribing a constant velocity, the ice flow follows a constant flux in two dimensions ($F_{\text{inlet}}(t)$).
- A lateral friction is prescribed to account for a constant fjord width of 10 km. This parametrization follows Gagliardini et al. (2010).

For the purpose of comparison, we chose to apply submarine melting and ice mélange forcing on glaciers in a quasi-steady-state (QSS) mode, i.e. their front has to stabilize within a given range, i.e., not more than the extent of one calving event. Among the 60 simulations generated by the LHS sampling, 23 had this feature, and are

TCD
9, 183–221, 2015

listed in Table 1. Other geometries either advanced too far without calving, or collapsed because of prolific calving. The sets of damage parameters with which a QSS was reached generally differed slightly from those calibrated in Krug et al. (2014). B ranged from 1.5 to 3 MPa^{-1}, and σ_{th} from 0.01 to 0.11 MPa (Compared with 0.5 to 2 MPa^{-1} and 0.01 to 0.2 MPa respectively, in Krug et al., 2014). The explanation for these differences is straightforward: the geometries studied here flow on a linear bedrock, with no bumps or roughness. Consequently, except near the front, no high velocity gradients appeared in the upper surface. Damage is consequently more difficult to initiate than in cases of rough bedrock, and consequently has to be promoted. In addition, since thinner glaciers are subject to less internal stress, they require parameters that promote damaging, unlike thicker glaciers (see Table 1).

For the sake of clarity, out of the 23 representative geometries, unless otherwise specified, in Sects. 4 and 5, we only use one to illustrate the model's response. This terminus-floating geometry (hereafter referred to as Geo. 12) is shown in bold in Table 1. However, the conclusions obtained in this study are robust against all the geometries considered, as discussed in Sects. 4.1 and 4.2.

3.2 Model experiments

The 23 setups summarized in Table 1 were run for seven years to reach the QSS discussed above (spin-up). After this spin-up, for each, we imposed eight perturbations in melting or ice mélange, as well as a control run (CR), in which the glacier continues its QSS evolution. These forcings were maintained for five years, after which they were removed, and we let the geometries evolve freely for five more years (relaxation period). In total, we performed 216 simulations of 17 years each.

The perturbations described in Sects. 3.2.1 and 3.2.2 are listed in Table 2. Perturbations in submarine frontal melting are named U1 to U4 (for "Undercutting"). Ice mélange perturbations are named S1 to S4 (for "Sikussak", the Greenlandic word for ice mélange).

TCD
9, 183–221, 2015

3.2.1 Submarine melting parameterization

Glacier frontal melting usually results from warm saline ocean water entering the fjord and mixing with fresh and cold glacier runoff. The resulting current melts the ice it meets as it rises along the calving face (Motyka et al., 2003). The melting intensity appears to be tightly linked with ocean water circulation, water stratification and its variability, as well as the specificities of the fjord, topography, size, or runoff seasonality (Straneo et al., 2011) and could partly explain the wide range of different measurements from one glacier to another. Rignot et al. (2010) measured summer melt rates ranging from 0.6 and 3.8 m day^{-1} at the face of four calving glaciers in West Greenland. Sutherland and Straneo (2012) calculated an annual mean melt rate of around 2 m day^{-1} in the area of the Sermilik Fjord – Helheim Glacier whereas Inall et al. (2014) measured summer values of around 10 m day^{-1} along the face of Kangerdlugssuaq Glacier, Southeast Greenland. Using a similar technique, in Alaska, Bartholomaus et al. (2013) obtained a range between 9 and 17 m day^{-1} for Yahtse Glacier, and Motyka et al. (2003) measured 12 m day^{-1} at the calving front of LeConte Glacier, in Alaska.

To our knowledge, most parameterizations of frontal melt in ice flow models published so far assume a linear variation of melt from 0 at sea level to a maximum value at the lowest point of the front. In what follows, this maximum value is used to characterize the intensity of the melt, and is referred to as *maximal melt rate* (MMR). Todd and Christoffersen (2014) applied a MMR of 8 m day^{-1} during three summer months and 0 m day^{-1} for the rest of the year. Cook et al. (2014) tested different values of MMR ranging from 2.7 to 13 m day^{-1} during the five month summer period and a winter constant MMR of 0.41 m day^{-1} (actually 150 m year^{-1}).

Following these studies and measurements, we tested different MMR summer values ranging from 0.41 to 12 m day^{-1}, following a four month sinusoidal peak and decay. In winter, following Cook et al. (2014), we prescribed a constant MMR of 0.41 m day^{-1} (see Fig. 2a). The melt rate was imposed in the front-normal direction, and its value is listed in Table 2. We deliberately chose to ignore melting at the bottom surface in

TCD
9, 183–221, 2015

the cases when the glacier started to float. We do not deny that this choice is a limitation, but we made it because we had no information on how the measured melt rate is distributed below the floating tongue and along the calving face. Considering that prescribing the same MMR under the glacier tongue would lead to its rapid collapse and that we wanted to compare the different behaviors of grounded and floating glaciers, taking into account melting under the tongue would require a more complex melting parameterization, which is beyond the scope of this study.

3.2.2 Ice mélange parameterization

Although ice mélange and its effect on glacier dynamics have been studied for a few decades (Rignot and MacAyeal, 1998; Reeh et al., 2001; Joughin et al., 2008c), two major unknowns remain: (i) the speed at which it freezes and melts and (ii) the force it applies against the glacier front.

(i) Seale et al. (2011) studied the correlation between ice mélange disintegration and front retreat in fjords in Greenland using MODIS imagery and showed that melting can occur in a very short time, from a few days to a couple of weeks, whereas sea ice stiffening can take much longer. However, due to the lack of solar illumination, they did not obtained reliable information regarding ice mélange freezing. We thus chose to simulate a growing period of five months followed by a 20 day decay period.

(ii) The question of the force transmitted up glacier by the ice mélange is more complex: using a 2-D flow line model, the back-force must be represented as pressure applied over a thickness. Measurements of the back-pressure $\sigma_{b_{max}}$ are difficult to obtain. The main studies inferred and used a broad range of values between [0.02; 3] MPa (Nick et al., 2009; Vieli and Nick, 2011; Walter et al., 2012; Cook et al., 2014; Todd and Christoffersen, 2014). To investigate glacier response to maximum back-pressure, we tested values up to 1 MPa. As 1 MPa is about the strength of pure ice under tension (Schulson and Duval, 2009), it represents an upper bound for $\sigma_{b_{max}}$. The mélange thickness h was broadly estimated within [70; 130] m in several studies (Fricker et al., 2005; Seneca Lindsey and Dupont, 2012; Cook et al., 2014; Todd and Christoffersen, 2014).

TCD
9, 183–221, 2015

Considering that sea ice binds fragments of icebergs together, we can reasonably assume its stiffness is the first-order control on mélange strength. Anderson (1961) linked the increase in sea ice thickness to the square root of the time and to the gradient between oceanic and atmospheric temperatures. Thus, considering sea ice strength to be closely correlated with its thickness and keeping the same kind of kinetics, we expressed the back-pressure applied by the mélange on the glacier as:

$$\sigma_b(t) = \begin{cases} \frac{\sigma_{b_{max}}}{\sqrt{150}}\sqrt{t} \pmod{365\,\text{days}} & \text{in winter} \\ \sigma_{b_{max}} - \frac{\sigma_{b_{max}}}{\sqrt{20}}\sqrt{t} \pmod{365\,\text{days}} & \text{at the end of winter} \\ 0 \pmod{365\,\text{days}} & \text{in summer} \end{cases} \quad (5)$$

Ice mélange growth and decay is depicted in Fig. 2b.

Finally, the ice mélange was prescribed through a time-varying back-stress assumed to be homogeneous over its thickness and resulting in a total back-force equal to the product $\sigma_b(t) \cdot h$. We tested several combinations of mélange thickness and back-pressure parameters, but for the rest of this study, we only illustrate the most representative (S1 to S4, see Table 2).

4 Results

4.1 Melting impact

The simulation starts on 1 January (time = 0), when the prescribed melt rate is set to its minimum value. The distribution of maximum melt rate for U1 to U4 and for the control run is given in Fig. 3a. The control run was not subject to any melt rate and its front position never moved by more than few tens of meters (see Fig. 3b). Figure 4 shows the shape of the glacier under perturbation U3 in the middle of the summer season (day 173). Simulations U1 to U4 produced slight oscillations, resulting in a slight advance of the terminus compared to the control run, but it never moved more than 400 m downstream. These advances may seem counterintuitive as most research suggests that

TCD
9, 183–221, 2015

submarine melting causes the front to retreat. However, our model revealed that when an advance takes place, it is not triggered by the same mechanism in all the setups. It is related to (i) a decrease in the frequency of calving events (this process is described in Sect. 5.2 below) and/or (ii) a torque effect caused by the retreat of the lowest point of the front (due to melting) and the advance of the highest point. In the case presented here, the advance of the front is due to a decrease in the frequency of calving events. Its geometry is illustrated in Fig. 4.

As soon as the forcing was removed, all the fronts reached their QSS position within a few months, except in simulation U4 (whose specific behavior is discussed in Sect. 5.2). The ice velocity at the front varied within a range of 200 m year^{-1}, which is very similar to the natural variation in the control run after a calving event (see Fig. 3.c).

Considering the contribution of melting and calving to ice loss, the volume of calved ice always appears to be larger than the melted volume. During summer, melting accounted for up to ∼ 23 % of the total mass loss (Fig. 5). Comparing winter and summer suggests that an increase in the intensity of undercutting does not significantly alter the total loss: more ice is melted but less ice is calved, meaning the cumulated volume does not vary significantly over the seasons.

To account for the different geometries, we summarized them as a function of their QSS mean thickness and velocity at the terminus for a given realistic forcing in melting (U2) (Fig. 6). The conclusions drawn above were qualitatively confirmed for all the other geometries: mean ice loss during the melting season was comparable to the ice loss during the rest of the year, whatever the size and velocity of the glacier. In summer, the calved volume was reduced by the increasing melt rate, but the cumulated loss remained unchanged.

4.2 Ice mélange impact

To measure the impact of ice mélange, we ran simulations S1 to S4 (Table 2), as well as the control run. Figure 7a shows the ice mélange intensity. Figure 7b shows changes in the position of the front as a function of time in the four corresponding experiments

TCD
9, 183–221, 2015

and in the control run (dashed black line). Two types of behavior were observed during the first five years. In winter, the ice mélange strengthened, and calving frequency decreased or stopped. As a consequence, the front advanced. In summer, the decay of the ice mélange back-force was immediately followed by a rapid sequence of large-scale iceberg calving events. In all the perturbation simulations, the glacier front was always located further downstream than in the control run. Each winter, the gaps between the positions of the S1–S4 fronts and that of the control run increased to reach a value of 500 m in S1 and 3 km in S4. Moreover, in perturbations S2, S3, and S4, after each year, the front did not retreat back to its QSS position, suggesting a consequence for inter-annual mass loss. These behaviors are consistent with observations, confirming the hypothesis that a strong mélange reduces calving discharge (Sohn et al., 1998; Joughin et al., 2008c).

Figure 7c shows the ice velocity at the front using the same color scale. The behavior of the terminus was inversely correlated with the velocity of the ice. The advance of the front in winter led to a decrease in ice velocity due to the increasing buttressing effect of the glacier sliding against the fjord walls and, to a lesser extent, to increasing back-pressure with increasing ice mélange strength (e.g. S3 and S4). As can be seen for the three highest back-forces (S2, S3, S4), when the mélange collapsed, the ice velocity at the front increased more than in the control run. The increase in speed can be explained by the following chronology. (i) First, the release of the mélange back-force accelerated the ice flow. (ii) Second, after the first calving event was triggered, the resulting geometry was a high vertical ice cliff. Velocity vectors were no longer parallel to the sea level and a torque appeared, leading to a force imbalance that further increased the ice velocity at the front. The red inset in Fig. 7 shows the first year of the forcing and underlines this phenomenon: at stage 1, mélange strength was maximum and its decay accelerated ice flow. At stage 2, the major front retreat in simulation S4 occurred, further accelerating the flow.

Such rapid acceleration of the flow was observed during calving events at the front of the Jakobshavn glacier in May 2007 by Amundson et al. (2008). Near the front, GPS

TCD
9, 183–221, 2015

stations recorded an increase in ice velocity from 11 315 to 12 775 m a^{-1} in 20 days, during which the glacier underwent three calving events that were attributed to an adjustment in the stress field. The freshly calved glacier was shorter, the buttressing effect was reduced and glacier flow accelerated (Benn et al., 2007b). Walter et al. (2012) monitored an increase in ice velocity up to 550 m a^{-1} during the days following the break up of the ice mélange at the terminus of Store Glacier. Our results are in agreement with these variations in measured velocity.

Figure 8 shows all the geometries for perturbation S2. Whatever the glacier geometry, the loss in summer was greater than in winter, as the winter ice mélange layer reduced calving activity. However, the same back-force do not have the same effect on small and large glaciers. In the case of smaller glaciers, it completely prevents calving; in the case of larger geometries, it only decreases the iceberg discharge. This explains why in the winter inset in Fig. 8, the thickest glaciers show the smallest contrast between winter and summer. This feature is also visible in Fig. 7b: large ice mélange intensities prevent calving (light blue, yellow and red curves), while smaller intensities simply reduce calving frequency (dark blue). This consideration reinforces the need for better knowledge of the properties of ice mélange.

5 Discussion

5.1 Mechanical impact of the ice mélange on the glacier front

According to Amundson et al. (2010), to prevent the rotation of a calved iceberg away from the terminus, the required back-force is between $\sim 1.0 \times 10^7$ and 10.0×10^7 N m^{-1}, depending on the glacier flotation and the inclination angle of the iceberg. To our knowledge, no study has suggested another effect of the ice mélange on the calving margin of tidewater outlet glaciers.

Concerning perturbations caused by the ice mélange, our model suggests that calving ceases as soon as the applied back-force reaches a given value. We investigated

TCD
9, 183–221, 2015

model sensitivity to the applied back-force by evaluating the value of this threshold. To this end, we isolated the pairs of parameters ($\sigma_{b_{max}}$, h) for which the winter season was characterized by the absence of calving events. For each of the five winter seasons, we then calculated the back-pressure applied when calving ceased, using Eq. (5). Multiplying this back-stress by the thickness of the ice mélange gives a back-force per meter of lateral width. The corresponding distribution for the 45 values is given in Fig. 9, whose the mean value is around $1.1 \times 10^7\,\mathrm{N\,m^{-1}}$.

Our coupled ice flow and calving model enabled us to distinguish between the different processes that culminate in iceberg calving that could be affected by the ice mélange. In the first stage, development of the crevasse field is determined by the damage criterion χ, which quantifies the incrementation of damage in the ice. Figure 10a shows changes in the position of the terminus over a period of 150 days, i.e. a full winter season. Three key events are highlighted by diamond symbols. The red diamond corresponds to a situation in which the glacier is about to calve, the yellow diamond illustrates a case where the glacier is subject to ice mélange, and the blue diamond corresponds to a situation in which the glacier has just calved. Figure 10b shows the value of χ along the upper surface where the tensile stress is the highest. During an ice mélange event (yellow curve), damage production is slightly lower than that in the pre- and post-calving situations, but remains positive. This means that ice mélange reduces the production of damage, but that the effect is too weak to completely halt damage to the ice.

Following damage to the ice, three criteria have to be fulfilled to trigger calving: the condition on damage contour $D = D_c$, the initiation of fracture propagation at a depth given by the D_c contour, and propagation at sea level. These criteria are shown in Fig. 10c, where the stress intensity factor is represented on the horizontal axis. The vertical extent of the thick colored lines shows the length of the damage envelope (the front is located at the top of the figure): a longer one illustrates a more extended crevasse field. As expected, the thick blue curve is almost nonexistent: as calving has just occurred, the glacier surface is not sufficiently damaged to calve again immediately.

TCD
9, 183–221, 2015

In contrast, the thick red and yellow lines show that the surface is sufficiently damaged to reach the criterion $D = D_c$ over a larger surface area. Wherever the stress intensity factor becomes higher than the ice toughness ($K_I > K_{Ic}$), crevasse propagation begins. This condition was satisfied in the case of the red and yellow lines near to the upper surface, so propagation can begin. The criterion $K_I > K_{Ia}$ must then be validated at sea level. The stress intensity at sea level is represented by the colored dashed curves. The red curve satisfies this criterion at some points, meaning that the calving event can begin. However, when the glacier undergoes the ice mélange layer (yellow dashed line), this criterion is not fulfilled, and as a consequence, the crevasse cannot propagate down to sea level.

Regarding model sensitivity to the thickness of the ice mélange, we observed that a thinner layer associated with a stronger back-force reduced the calving rate more than a thicker layer associated with a weaker back-force, with the same total back-force (data not shown). This is because the thinnest layer of ice mélange is concentrated at sea level which significantly reduces the stress intensity factor at this depth, thereby preventing crevasse propagation.

These mechanisms could explain the behavior observed in Fig. 7b. For simulations S2, S3 and S4, the figure shows that the decay of the mélange layer was followed by a "cascade" of calving events. However, the glacier did not immediately retreat to its QSS position. This rate of retreat depends on the amount of damage at the surface, which depends directly on the driving force of the ice mélange. This suggests that a stronger or longer winter season could alter the position of the front over a period of more than one year, if one consider the "stress history" of the glacier, and does not only rely on a one-off record of the stress balance.

The results presented in this section are in direct contrast with those of Cook et al. (2014). These authors observed no remarkable changes in the position of the front unless they applied a back-force of $50.0 \times 10^7\,\mathrm{N\,m^{-1}}$, even if they simulated a difference of 25 m in the longitudinal extent of the crevasse around the front for smaller values of ice mélange ($5.0 \times 10^7\,\mathrm{N\,m^{-1}}$). Conversely, Todd and Christoffersen (2014)'s results

TCD
9, 183–221, 2015

clearly agree with ours, as they simulated a comparable advance of the front (∼1.5 km) with a back-force close to ours in simulation S2. Finally, for an applied force of the same order of magnitude, our model shows that the ice mélange acts sooner than suggested by Amundson et al. (2010) by preventing the propagation of the fracture down to the glacier base.

5.2 Differences between floating and grounded termini

Figure 11a shows the maximum difference in the surface along-flow component of the deviatoric stress tensor S_{xx} between the CR and the U2 simulations, in the vicinity of the front (< 600 m) during the middle of the first summer period. Undercutting grounded glaciers slightly increased the tensile stress at the upper surface (red dots). It increased the frequency of calving events, but reduced the size of each event (see red dots and crosses in Fig. 11b). Conversely, in the case of floating glaciers, the surface adjustment of the tongue decreased the tensile stress compared with the control run (Fig. 11a, blue dots). Consequently, the frequency of calving events decreased slightly, but the distance the front retreated at each event increased slightly (blue dots and crosses in Fig. 11b).

Concerning the behavior of the grounded geometry of Helheim Glacier, Cook et al. (2014) stated that the melting of the front has relatively little effect on the position of the front, unless the prescribed melt rates are extremely high (up to 20 m day^{-1}). On Store Glacier, Todd and Christoffersen (2014) modelled a slight increase in frequency with undercutting, as well as a decrease in the amplitude of the retreat of the calving front, and they attributed this inter-annual stability to the glacier's topographic setting. As Todd and Christoffersen (2014)'s geometry was grounded when the frontal melting was prescribed, their modelling results are in agreement with ours.

In our simulations, another difference appeared between grounded and floating glaciers. In Sect. 4, we showed that for most perturbations, after the relaxation period, glacier fronts usually reached their QSS position. However, this was not the case for the glacier undergoing perturbation U4 illustrated in Fig. 3b. Indeed, its front rapidly

TCD
9, 183–221, 2015

advanced further downstream than the others, and appeared to stabilize at an extent of 6.2 km, compared with 6.0 km for the other fronts. When extended to other geometries, the same result also was obtained in some of the ice mélange experiments. However, it only concerned glaciers with a floating tongue, and only occurred under the strongest forcings.

Concerning these processes, we propose an explanation for this phenomenon (see Fig. 12). The melting perturbation applied on the glacier front affects the shape of the floating tongue (Fig. 12b). It reduces its area along with the subsequent buttressing effect. As a consequence, the whole glacier accelerates, thins, and the grounding line retreats (Fig. 12c). The ice flux at the grounding line is therefore modified, and a new equilibrium is established that relies on interactions between the ice flow, damage production, and the calving law. Considering the ice mélange, the concept is similar but the process is reversed (Fig. 12d). As the ice mélange prevents the floating tongue from calving, the area of the tongue increases. Consequently, the glacier slows down, thickens, and the grounding line advances (Fig. 12e). Again, a new equilibrium may be established, with an associated quasi-steady state front dynamics.

6 Conclusions

Ice mélange and melting of the glacier front have been reported by many authors to influence the behavior of tidewater glaciers. In particular, they have been cited as a possible explanation for the seasonal advance and retreat cycles of glacier fronts, among other external forcings. However, although some correlations between these mechanisms and the advance/retreat of the front have been established on many outlet glaciers in Greenland, little is known about the exact role of these forcings.

In this study, we combined a full-Stokes ice flow model with a calving framework using damage and fracture mechanics to investigate the impact of these forcings on glacier dynamics. This allowed us to represent the slow degradation of the mechanical properties of the ice, and the initiation and propagation of pre-existing fractures, which

TCD
9, 183–221, 2015

are essential to describe the processes occurring at the front. We performed experiments on a large set of synthetic geometries using different values for melting and ice mélange back-stress and thickness, and the conclusions we have drawn are robust in all these experiments.

Our modelling showed that melting has an impact on the calving rate and on the position of the front (less than a few hundred meters), but no effect on inter-/pluri-annual mass loss. On the contrary, applying an ice mélange layer against the front affects its position to a larger extent (up to several kilometers) compared to melting. In addition, its consequences for the inter-/pluri-annual mass loss, if slight, may not be completely negligible and thus support Joughin et al. (2008c)'s statement, according to whom "It is likely that the processes that control the seasonal calving cycle may also influence the inter annual variability". By investigating the processes occurring during calving events, we have shown that the ice mélange first reduces the rate of surface damage by reducing the tensile stress in the glacier upper surface, and second, prevents fracture propagation at sea level and hence calving. Better field characterization of undercutting and ice mélange properties should increase the accuracy of further modelling.

Finally, our results also reveal a feature that is specific to glaciers with floating termini, i.e., that strong perturbations (either in melting or in ice mélange) may affect their pluri-annual behavior. By affecting the buttressing effect of the tongue, the perturbation may modify the subsequent glacier equilibrium and lead to a new stable geometry for the same model parameters. This new stable position then depends on feedback between glacier flow and calving law parameters.

Acknowledgements. This study was funded by the Agence Nationale pour la Recherche (ANR) through the SUMER, Blanc SIMI 6 – 2012. All the computations presented in this paper were performed using the CIMENT infrastructure (https://ciment.ujf-grenoble.fr), which is supported by the Rhône-Alpes region (GRANT CPER07_13 CIRA:(http://www.ci-ra.org). We also thank the CSC-IT Center for Science Ltd (Finland) for their support in Elmer/Ice development.

TCD
9, 183–221, 2015

References

Amundson, J., Truffer, M., Lüthi, M., Fahnestock, M., West, M., and Motyka, R.: Glacier, fjord, and seismic response to recent large calving events, Jakobshavn Isbræ, Greenland, Geophys. Res. Lett., 35, L22501, doi:10.1029/2008GL035281, 2008. 196

Amundson, J. M., Fahnestock, M., Truffer, M., Brown, J., Lüthi, M. P., and Motyka, R. J.: Ice mélange dynamics and implications for terminus stability, Jakobshavn Isbræ, Greenland, J. Geophys. Res., 115, F01005, doi:10.1029/2009JF001405, 2010. 186, 197, 200

Anderson, D. L.: Growth rate of sea ice, J. Glaciol., 3, 1170–1172, 1961. 194

Bartholomaus, T. C., Larsen, C. F., and O'Neel, S.: Does calving matter? Evidence for significant submarine melt, Earth Planet. Sc. Lett., 380, 21–30, 2013. 186, 192

Benn, D. I., Hulton, N. R., and Mottram, R. H.: 'Calving laws','sliding laws' and the stability of tidewater glaciers, Ann. Glaciol., 46, 123–130, 2007a. 186

Benn, D. I., Warren, C. R., and Mottram, R. H.: Calving processes and the dynamics of calving glaciers, Earth-Sci. Rev., 82, 143–179, 2007b. 186, 197

Cazenave, A.: How fast are the ice sheets melting?, Science, 314, 1250–1252, 2006. 185

Church, J., Clark, P., Cazenave, A., Gregory, J., Jevrejeva, S., Levermann, A., Merrifield, M., Milne, G., Nerem, R., Nunn, P., Payne, A., Pfeffer, W., Stammer, D., and Unnikrishnan, A.: Sea Level Change, in: Climate Change 2013: The Physical Science Basis. Contribution of Working Group I to the Fifth Assessment Report of the Intergovernmental Panel on Climate Change, edited by: Stocker, T., Qin, D., Plattner, G.-K., Tignor, M., Allen, S., Boschung, J., Nauels, A., Xia, Y., Bex, V., and Midgley, P., Cambridge University Press, Cambridge, United Kingdom and New York, NY, USA, 2013. 184

Cook, S., Rutt, I. C., Murray, T., Luckman, A., Zwinger, T., Selmes, N., Goldsack, A., and James, T. D.: Modelling environmental influences on calving at Helheim Glacier in eastern Greenland, The Cryosphere, 8, 827–841, doi:10.5194/tc-8-827-2014, 2014. 186, 187, 192, 193, 199, 200

Copland, L., Mueller, D. R., and Weir, L.: Rapid loss of the Ayles ice shelf, Ellesmere Island, Canada, Geophys. Res. Lett., 34, L21501, doi:10.1029/2007GL031809, 2007. 186

Durand, G., Gagliardini, O., De Fleurian, B., Zwinger, T., and Le Meur, E.: Marine ice sheet dynamics: Hysteresis and neutral equilibrium, J. Geophys. Res.-Earth, 114, F03009, doi:10.1029/2008JF001170, 2009. 190

TCD
9, 183–221, 2015

Fricker, H., Young, N., Coleman, R., Bassis, J., and Minster, J.-B.: Multi-year monitoring of rift propagation on the Amery Ice Shelf, East Antarctica, Geophys. Res. Lett., 32, L02502, doi:10.1029/2004GL021036, 2005. 186, 193

Gagliardini, O., Durand, G., Zwinger, T., Hindmarsh, R., and Le Meur, E.: Coupling of ice-shelf melting and buttressing is a key process in ice-sheets dynamics, Geophys. Res. Lett., 37, L14501, doi:10.1029/2010GL043334, 2010. 190

Heinke, J., Ostberg, S., Schaphoff, S., Frieler, K., Müller, C., Gerten, D., Meinshausen, M., and Lucht, W.: A new climate dataset for systematic assessments of climate change impacts as a function of global warming, Geosci. Model Dev., 6, 1689–1703, doi:10.5194/gmd-6-1689-2013, 2013. 188, 189

Higgins, A. K.: North Greenland glacier velocities and calf ice production, Polarforschung, 60, 1–23, 1991. 186

Holland, D. M., Thomas, R. H., De Young, B., Ribergaard, M. H., and Lyberth, B.: Acceleration of Jakobshavn Isbrae triggered by warm subsurface ocean waters, Nat. Geosci., 1, 659–664, 2008. 185

Howat, I. M., Ahn, Y., Joughin, I., van den Broeke, M. R., Lenaerts, J., and Smith, B.: Mass balance of Greenland's three largest outlet glaciers, 2000–2010, Geophys. Res. Lett., 38, doi:10.1029/2011GL047565, 2011. 185

Inall, M. E., Murray, T., Cottier, F. R., Scharrer, K., Boyd, T. J., Heywood, K. J., and Bevan, S. L.: Oceanic heat delivery via Kangerdlugssuaq Fjord to the south-east Greenland ice sheet, J. Geophys. Res.-Oceans, 119, 631–645, 2014. 186, 192

Joughin, I., Das, S. B., King, M. A., Smith, B. E., Howat, I. M., and Moon, T.: Seasonal speedup along the western flank of the Greenland Ice Sheet, Science, 320, 781–783, 2008a. 186

Joughin, I., Howat, I., Alley, R. B., Ekstrom, G., Fahnestock, M., Moon, T., Nettles, M., Truffer, M., and Tsai, V. C.: Ice-front variation and tidewater behavior on Helheim and Kangerdlugssuaq Glaciers, Greenland, J. Geophys. Res.-Earth, 113, F01004, doi:10.1029/2007JF000837, 2008b. 186

Joughin, I., Howat, I. M., Fahnestock, M., Smith, B., Krabill, W., Alley, R. B., Stern, H., and Truffer, M.: Continued evolution of Jakobshavn Isbrae following its rapid speedup, J. Geophys. Res.-Earth, 113, F04006, doi:10.1029/2008JF001023, 2008c. 186, 193, 196, 202

Khan, S. A., Wahr, J., Bevis, M., Velicogna, I., and Kendrick, E.: Spread of ice mass loss into northwest Greenland observed by GRACE and GPS, Geophys. Res. Lett., 37, L06501, doi:10.1029/2010GL042460, 2010. 185

TCD
9, 183–221, 2015

Khan, S. A., Kjaer, K. H., Bevis, M., Bamber, J. L., Wahr, J., Kjeldsen, K. K., Bjork, A. A., Korsgaard, N. J., Stearns, L. A., van den Broeke, M. R., Liu, L., Larsen, N. K., and Muresan, I. S.: Sustained mass loss of the northeast Greenland ice sheet triggered by regional warming, Nature Clim. Change, advance online publication, 4, 292–299, doi:10.1038/nclimate2161, 2014. 185

Khazendar, A. and Jenkins, A.: A model of marine ice formation within Antarctic ice shelf rifts, J. Geophys. Res.-Oceans, 108, p. 28, doi:10.1029/2002JC001673, 2003. 186

Krug, J., Weiss, J., Gagliardini, O., and Durand, G.: Combining damage and fracture mechanics to model calving, The Cryosphere, 8, 2101–2117, doi:10.5194/tc-8-2101-2014, 2014. 189, 190, 191

Motyka, R. J., Hunter, L., Echelmeyer, K. A., and Connor, C.: Submarine melting at the terminus of a temperate tidewater glacier, LeConte Glacier, Alaska, USA, Ann. Glaciol., 36, 57–65, 2003. 186, 192

Nick, F. M., Vieli, A., Howat, I. M., and Joughin, I.: Large-scale changes in Greenland outlet glacier dynamics triggered at the terminus, Nat. Geosci., 2, 110–114, 2009. 186, 193

Nick, F. M., van der Veen, C. J., Vieli, A., and Benn, D. I.: A physically based calving model applied to marine outlet glaciers and implications for the glacier dynamics, J. Glaciol., 56, 781–794, 2010. 186, 187

O'Leary, M. and Christoffersen, P.: Calving on tidewater glaciers amplified by submarine frontal melting, The Cryosphere, 7, 119–128, doi:10.5194/tc-7-119-2013, 2013. 186

Reeh, N., Thomsen, H. H., Higgins, A. K., and Weidick, A.: Sea ice and the stability of north and northeast Greenland floating glaciers, Ann. Glaciol., 33, 474–480, 2001. 186, 193

Rignot, E. and MacAyeal, D. R.: Ice-shelf dynamics near the front of Filchner-Ronne Ice Shelf, Antarctica, revealed by SAR interferometry, J. Glaciol., 44, 405–418, 1998. 193

Rignot, E., Box, J., Burgess, E., and Hanna, E.: Mass balance of the Greenland ice sheet from 1958 to 2007, Geophys. Res. Lett., 35, L20502, doi:10.1029/2008GL035417, 2008. 185

Rignot, E., Koppes, M., and Velicogna, I.: Rapid submarine melting of the calving faces of West Greenland glaciers, Nat. Geosci., 3, 187–191, 2010. 186, 192, 215

Rignot, E., Velicogna, I., Van den Broeke, M., Monaghan, A., and Lenaerts, J.: Acceleration of the contribution of the Greenland and Antarctic ice sheets to sea level rise, Geophys. Res. Lett., 38,L05503, doi:10.1029/2011GL046583, 2011. 185

TCD
9, 183–221, 2015

Schrama, E. J. and Wouters, B.: Revisiting Greenland ice sheet mass loss observed by GRACE, J. Geophys. Res.-Sol. Ea., 116, B02407, doi:10.1029/2009JB006847, 2011. 184, 185

Schulson, E. M. and Duval, P.: Creep and Fracture of Ice, Cambridge University Press, Cambridge, 2009. 193

Seale, A., Christoffersen, P., Mugford, R. I., and O'Leary, M.: Ocean forcing of the Greenland Ice Sheet: calving fronts and patterns of retreat identified by automatic satellite monitoring of eastern outlet glaciers, J. Geophys. Res.-Earth, 116, F03013, doi:10.1029/2010JF001847, 2011. 185, 193

Seneca Lindsey, D. and Dupont, T. K.: Mechanical effect of mélange-induced buttressing on embayment-terminating glacier dynamics, The Cryosphere Discuss., 6, 4123–4136, doi:10.5194/tcd-6-4123-2012, 2012. 193

Shepherd, A., Ivins, E. R., Geruo, A., Barletta, V. R., Bentley, M. J., Bettadpur, S., Briggs, K. H., Bromwich, D. H., Forsberg, R., Galin, N., Horwath, M., Jacobs, S., Joughin, I., King, M. A., Lenaerts, J. T. M., Li, J., Ligtenberg, S. R. M., Luckman, A., Luthcke, S. B., McMillan, M., Meister, R., Milne, G., Mouginot, J., Muir, A., Nicolas, J. P., Paden, J., Payne, A. J., Pritchard, H., Rignot, E., Rott, H., Sandberg Sørensen, L., Scambos, T. A., Scheuchl, B., Schrama, E. J. O., Smith, B., Sundal, A. V., van Angelen, J. H., van de Berg, W. J., van den Broeke, Michiel R. Vaughan, D. G., Velicogna, I., Wahr, J., Whitehouse, P. L., Wingham, D. J., Yi, D., Young, D., and Zwally, H. J.: A reconciled estimate of ice-sheet mass balance, Science, 338, 1183–1189, 2012. 184

Sohn, H.-G., Jezek, K. C., and Van der Veen, C.: Jakobshavn Glacier, West Greenland: 30 years of spaceborne observations, Geophys. Res. Lett., 25, 2699–2702, 1998. 186, 196

Straneo, F., Hamilton, G. S., Sutherland, D. A., Stearns, L. A., Davidson, F., Hammill, M. O., Stenson, G. B., and Rosing-Asvid, A.: Rapid circulation of warm subtropical waters in a major glacial fjord in East Greenland, Nat. Geosci., 3, 182–186, 2010. 185

Straneo, F., Curry, R. G., Sutherland, D. A., Hamilton, G. S., Cenedese, C., Våge, K., and Stearns, L. A.: Impact of fjord dynamics and glacial runoff on the circulation near Helheim Glacier, Nat. Geosci., 4, 322–327, 2011. 192

Sutherland, D. and Straneo, F.: Estimating ocean heat transports and submarine melt rates in Sermilik Fjord, Greenland, using lowered acoustic Doppler current profiler (LADCP) velocity profiles, Ann. Glaciol., 53, 50, doi:10.3189/2012AoG60A050, 2012. 186, 192

TCD
9, 183–221, 2015

Todd, J. and Christoffersen, P.: Are seasonal calving dynamics forced by buttressing from ice mélange or undercutting by melting? Outcomes from full-Stokes simulations of Store Gletscher, West Greenland, The Cryosphere Discuss., 8, 3525–3561, doi:10.5194/tcd-8-3525-2014, 2014. 186, 187, 192, 193, 199, 200

van den Broeke, M., Bamber, J., Ettema, J., Rignot, E., Schrama, E., van de Berg, W. J., van Meijgaard, E., Velicogna, I., and Wouters, B.: Partitioning recent Greenland mass loss, Science, 326, 984–986, 2009. 185

Vieli, A. and Nick, F.: Understanding and modelling rapid dynamic changes of tidewater outlet glaciers: issues and implications, Surv. Geophys., 32, 437–458, 2011. 187, 193

Vieli, A., Jania, J., and Kolondra, L.: The retreat of a tidewater glacier: observations and model calculations on Hansbreen, Spitsbergen, J. Glaciol., 48, 592–600, 2002. 186

Walter, J. I., Box, J. E., Tulaczyk, S., Brodsky, E. E., Howat, I. M., Ahn, Y., and Brown, A.: Oceanic mechanical forcing of a marine-terminating Greenland glacier, Ann. Glaciol., 53, 181–192, 2012. 186, 187, 193, 197

TCD
9, 183–221, 2015

Table 1. List of geometries and their associated parameters used for the model experiments. $\overline{H}_T$ refers to the QSS mean ice thickness of the terminus, F_{inlet} represents the ice flux at the inlet boundary and $\overline{H}_{w_T}$ is the QSS mean water depth at the terminus. $\overline{H}_{AB}$ is the mean height above buoyancy at the front, where the terminus is grounded. The letter F is used instead of $\overline{H}_{AB}$ if the glacier is afloat. σ_{th} is the stress threshold that starts damagen, B is the damage enhancement factor and D_c the damage contour. The line in bold is the representative simulation.

Geometry	$\overline{H}_T$ (m)	F_{inlet} ($\times 10^3$ m^2 a^{-1})	$\overline{H}_{w_T}$	$\overline{H}_{AB}$ (m)	σ_{th} (MPa)	B (MPa^{-1})	D_c (m)
Geo 1	358	710	308	16	0.017	2.9	0.47
Geo 2	356	679	307	14	0.014	1.6	0.42
Geo 3	362	488	319	7	0.025	1.8	0.44
Geo 4	342	446	297	12	0.037	2.3	0.41
Geo 5	354	626	306	14	0.031	2.6	0.45
Geo 6	362	572	317	10	0.041	2.2	0.46
Geo 7	348	610	300	15	0.054	2.8	0.46
Geo 8	456	1210	405	6	0.026	2.9	0.41
Geo 9	474	1133	427	F	0.021	1.5	0.44
Geo 10	465	1528	412	8	0.013	1.8	0.43
Geo 11	461	1432	409	7	0.037	2.2	0.41
Geo 12	**631**	**3940**	**623**	**F**	**0.059**	**2.4**	**0.54**
Geo 13	638	4406	632	F	0.024	2.1	0.6
Geo 14	597	2273	609	F	0.068	2.1	0.48
Geo 15	627	3535	632	F	0.021	1.7	0.53
Geo 16	824	7719	908	F	0.047	2.3	0.5
Geo 17	810	7143	909	F	0.050	1.6	0.41
Geo 18	860	10 203	975	F	0.032	1.5	0.48
Geo 19	842	8953	970	F	0.079	2.0	0.56
Geo 20	863	11 078	923	F	0.068	2.0	0.41
Geo 21	866	11 389	942	F	0.016	2.2	0.59
Geo 22	854	9979	942	F	0.115	2.4	0.43
Geo 23	810	7233	924	F	0.100	1.9	0.46

TCD
9, 183–221, 2015

Table 2. Complete list of the experiments performed for each setup listed in Table 1. Runs U1 to U4 refer to the undercutting experiments. The maximal melt rate is indicated by MMR. Runs S1 to S4 refer to the ice mélange experiments: $\sigma_{b_{max}}$ is the maximum ice mélange back-pressure applied over a depth h, and results in a maximum back-force of $\max(\sigma_b(t) \cdot h)$. The control run did not undergo either ice mélange or melting. For each forcing, the "realistic" cases are in bold.

Name run	$\sigma_{b_{max}}$ (kPa)	h (m)	$\max(\sigma_b(t) \cdot h)$ ($\times 10^7$ N m^{-1})	MMR (m day^{-1})
U1	0	0	0.0	3
U2	**0**	**0**	**0.0**	**6**
U3	0	0	0.0	9
U4	0	0	0.0	12
S1	170	80	1.36	0
S2	**200**	**100**	**2.0**	**0**
S3	350	120	4.2	0
S4	750	80	6.0	0
CR	0	0	0.0	0

TCD
9, 183–221, 2015

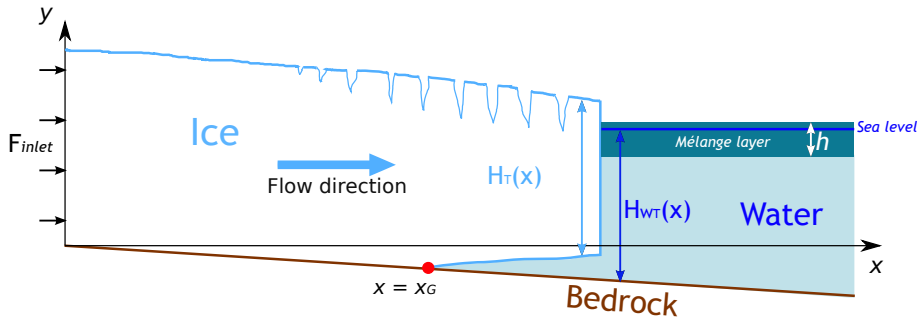

Figure 1. Setup of the experiment. $H_T(x)$, $H_{w_T}(x)$ and h represent glacier thickness, water depth, and ice mélange thickness, respectively. The glacier is grounded on a solid bedrock with a slightly positive slope (exaggerated here) represented by the thick brown line. The grounding line is indicated by the red dot, at the abscissa $x = x_G$. The blue arrow shows the direction of the ice flow.

TCD
9, 183–221, 2015

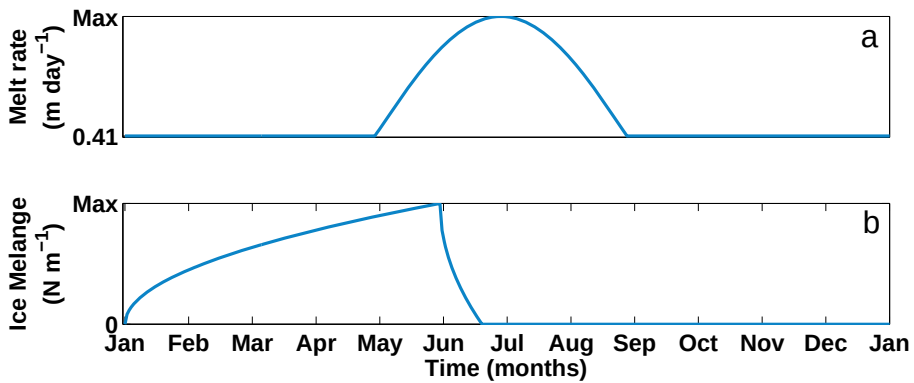

Figure 2. Shape of perturbations over a period of one year. **(a)** Melting parameterization at glacier bottom. **(b)** Ice mélange parameterization.

TCD
9, 183–221, 2015

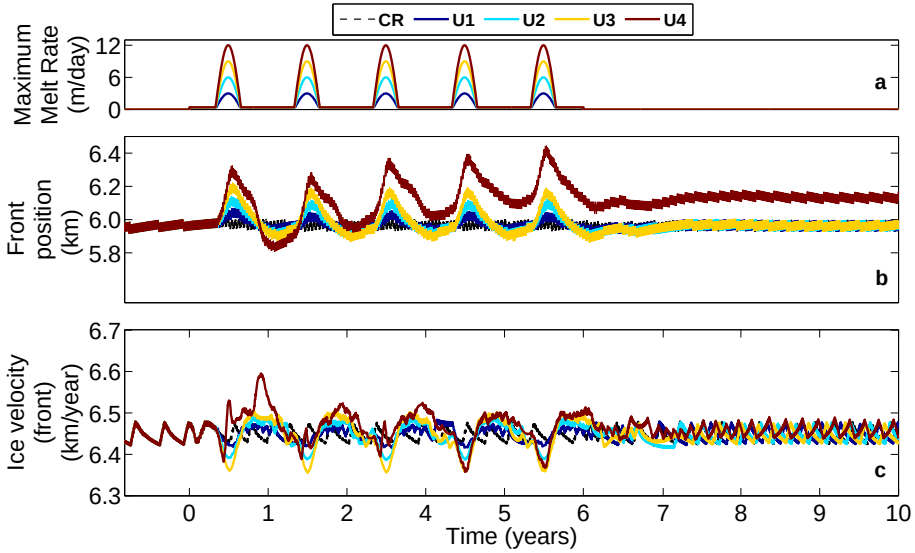

Figure 3. Glacier response in the undercutting experiments (Geo. 12, Table 2) U1 to U4 (colored lines) and CR (dashed black line). **(a)** Variation in the maximum melt rate imposed at the bottom surface of the glacier front. During the five month summer season, melting follows a sinusoidal pattern. Otherwise, a constant melt rate of 0.41 m day^{-1} is prescribed. **(b)** Variation in the position of the front as a function of time and **(c)** Ice velocity at the terminus. For the sake of clarity, the velocity was smoothed with a 10 day moving average.

TCD
9, 183–221, 2015

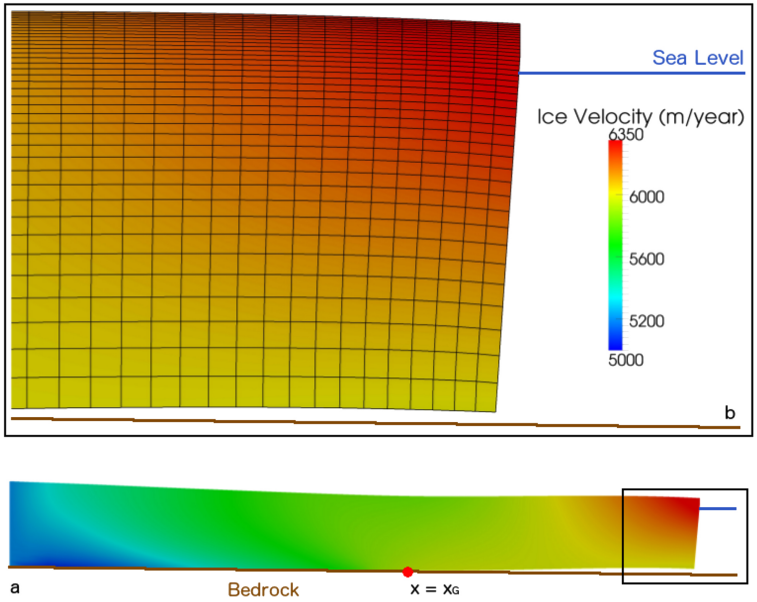

Figure 4. (a) Velocity field for the representative geometry (Geo. 12, Table 2), undergoing perturbation U3 at day 173 (first summer season). The red dot shows the position of the grounding line. **(b)** Zoom in the black rectangle, glacier front geometry and mesh.

TCD
9, 183–221, 2015

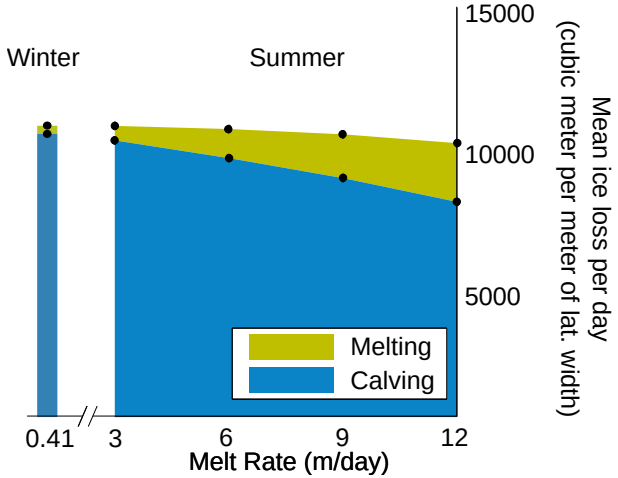

Figure 5. Mean daily winter and summer ice loss due to calving (blue) and melting (green) for five values of melt rate, over five years. Computed from the control run (CR) and Geo. 12, perturbations U1 to U4.

TCD
9, 183–221, 2015

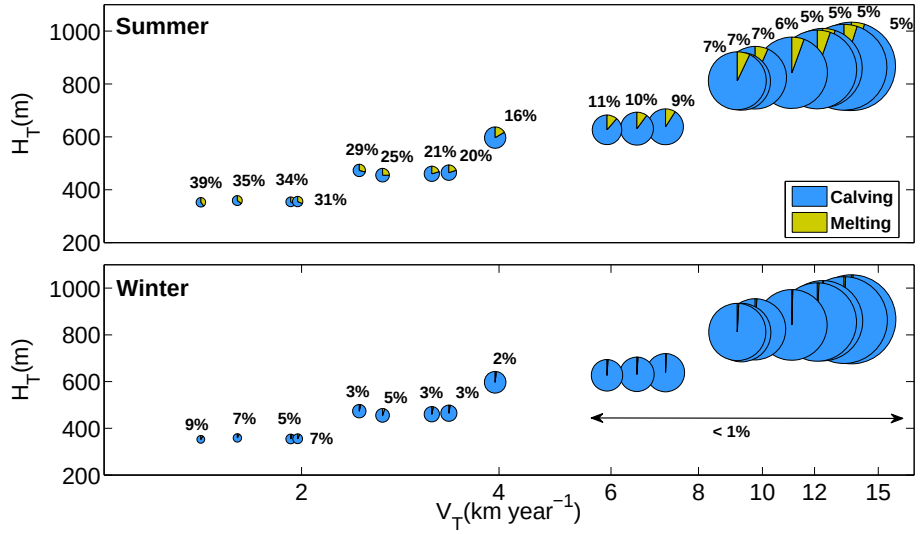

Figure 6. Cumulated ice loss (over 5 years) for the setups listed in Table 2, for experiment U2. The disks represent the volume of ice lost by the glacier associated with a mean ice front velocity $\overline{V}_T$ and ice front thickness $\overline{H}_T$. The figure distinguishes between the summer season (top) and the winter season (bottom). The fraction of ice loss due to melting is in green (also indicated by the percentage) and the fraction due to calving is in blue. To enable comparison between summer and winter, the volume is normalized daily. In summer, the melted fraction accounts for 5 to 39 % of the summer glacier loss (highest for smaller glacier), and agrees with the lower bounds of Rignot et al. (2010)'s calculations, especially for thinnest glaciers.

TCD
9, 183–221, 2015

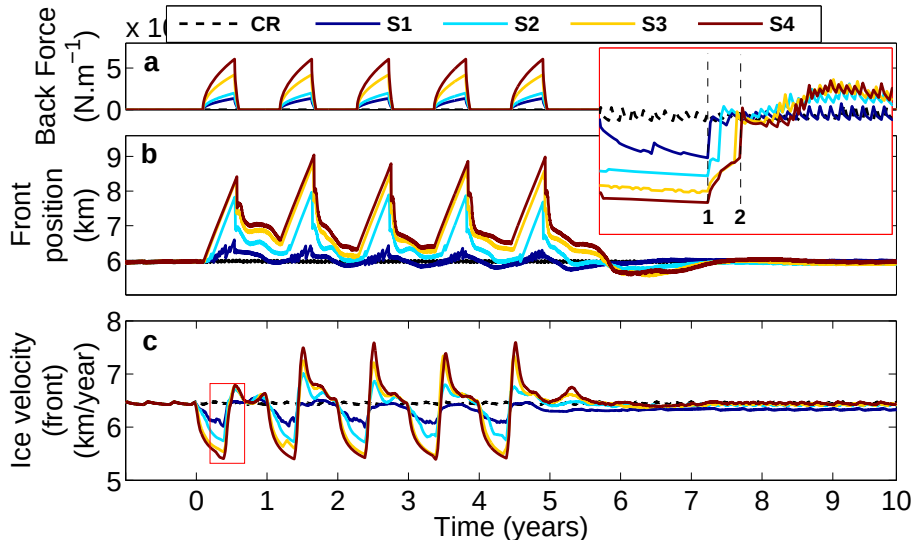

Figure 7. Glacier response in ice mélange experiments (Geo. 12, Table 2) S1 to S4 (colored lines) and in the control run (CR) (dashed black line). **(a)** Variation in mélange back-force $\sigma_b(t)*h$ as a function of time (per meter lateral width) . The value of the maximal back-force depends on the pairs of parameters ($\sigma_{b_{max}}$, h). **(b)** Variation in the position of the front as a function of time and **(c)** Ice velocity at the terminus. For the sake of clarity, velocity is smoothed with a 10-day moving average. The red inset shows the ice velocity at the terminus without smoothing, and the precise chronology of variations in velocity: the dashed vertical line 1 corresponds to the maximum mélange strength and line 2 corresponds to the major calving event in experiment S4.

TCD
9, 183–221, 2015

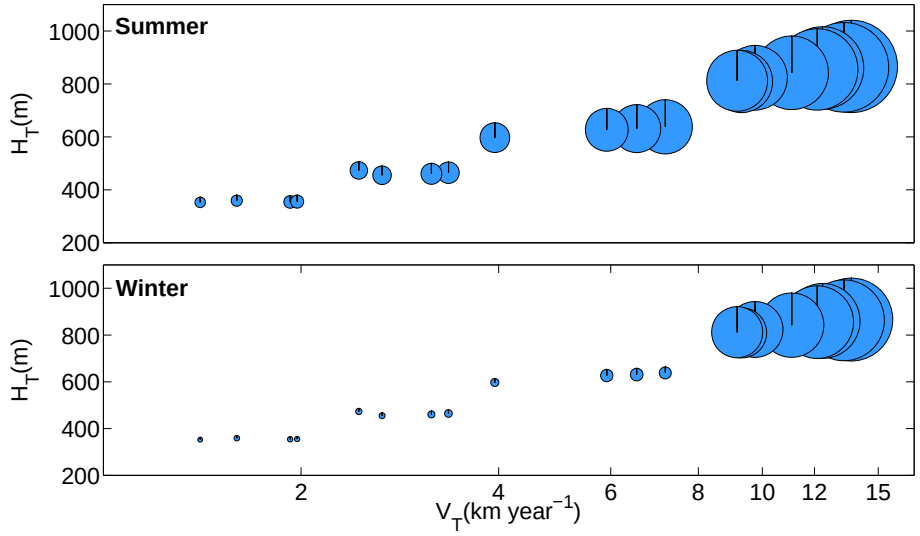

Figure 8. Cumulated ice loss (over 5 years) for the setups listed in Table 2, in experiment S2. The disks represents the volume of ice lost by the glacier associated with a mean ice front velocity $\overline{V}_T$ and ice front thickness $\overline{H}_T$. The figure distinguishes between summer season (at the top) and the winter season (at the bottom). To enable comparison between summer and winter, the volume is normalized daily.

TCD
9, 183–221, 2015

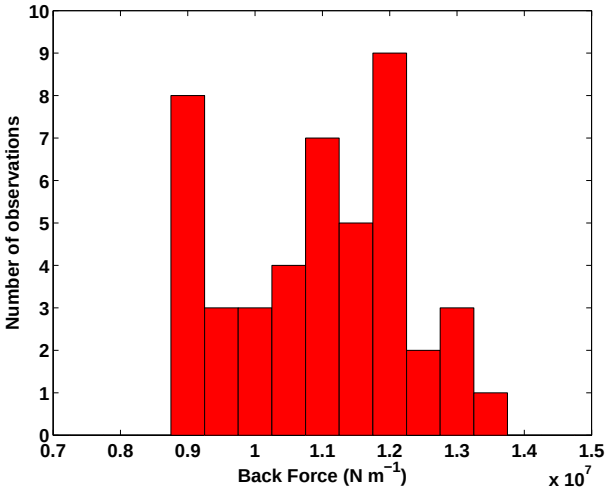

Figure 9. Histogram of the back-force from an ice mélange required to prevent calving. The mean of the distribution is $1.1 \times 10^7\,\mathrm{N\,m^{-1}}$ and its SD is $1.3 \times 10^6\,\mathrm{N\,m^{-1}}$, per meter of lateral width.

TCD
9, 183–221, 2015

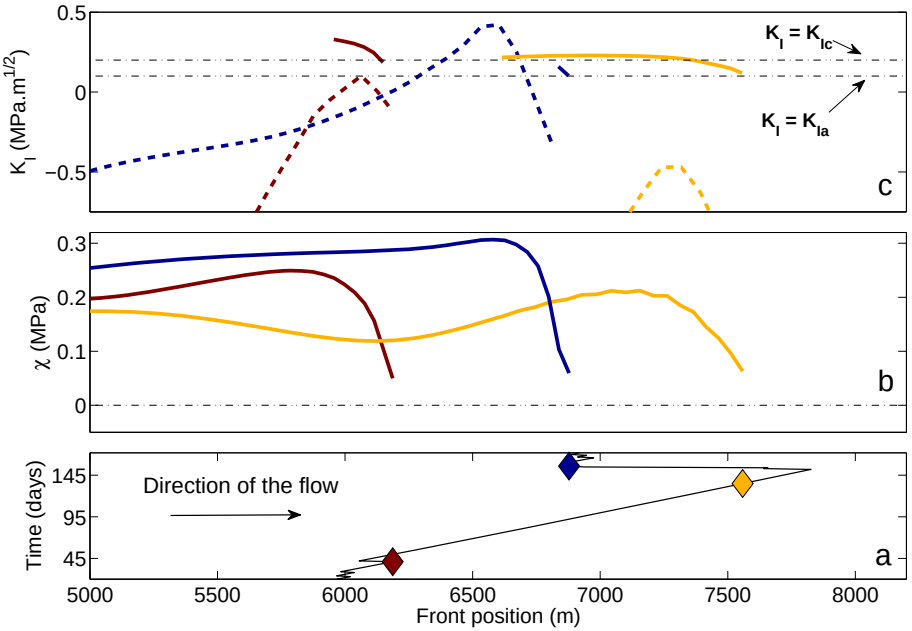

Figure 10. (a) Changes in the position of the front over a winter season for a glacier undergoing an ice mélange characterized by a back-stress $\sigma_{b_{max}} = 0.2$ MPa and a thickness $h = 100$ m. Red, yellow, and blue diamonds refer to days 46 (before winter season, before a calving event), 140 (during the winter season), and 161 (after the winter season, after a calving event), respectively. **(b)** Variation in the damage criterion χ at the upper surface along the flow-line using the same color code. **(c)** Variation in the stress intensity factor. Colored curves show the stress intensity factor computed at the depth at which the damage threshold $D = D_c$ is reached (thick curves) and at sea level (dashed curves). The horizontal dashed black lines represent ice toughness $K_{Ic} = 0.2\,\mathrm{MPa\,m^{-1}}$ and arrest criterion $K_{Ia} = 0.1\,\mathrm{MPa\,m^{-1}}$.

TCD
9, 183–221, 2015

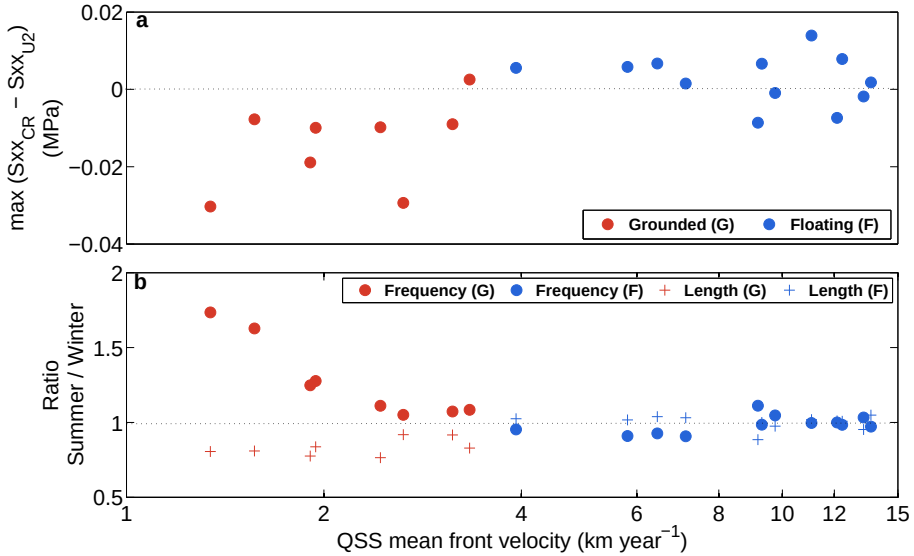

Figure 11. (a) Maximum difference in the along-flow component of the deviatoric stress tensor at the glacier surface for each glacier listed in Table 1 between the control run (CR) and the U2 experiment. The difference is computed within the 600 last meters before the calving front in the middle of the first summer (day 182). Red dots indicate grounded fronts, while blue dots highlight floating termini. **(b)** Ratio between summer and winter events for all the geometries listed in Table 1 forced by the U2 experiment (maximum melt rate: 6 m day^{-1}), as a function of the inlet flux. Grounded glaciers are in red, floating glaciers in blue. Circles and crosses refer to the mean number of calving events and to the mean length of the front retreat ratios, respectively.

TCD
9, 183–221, 2015

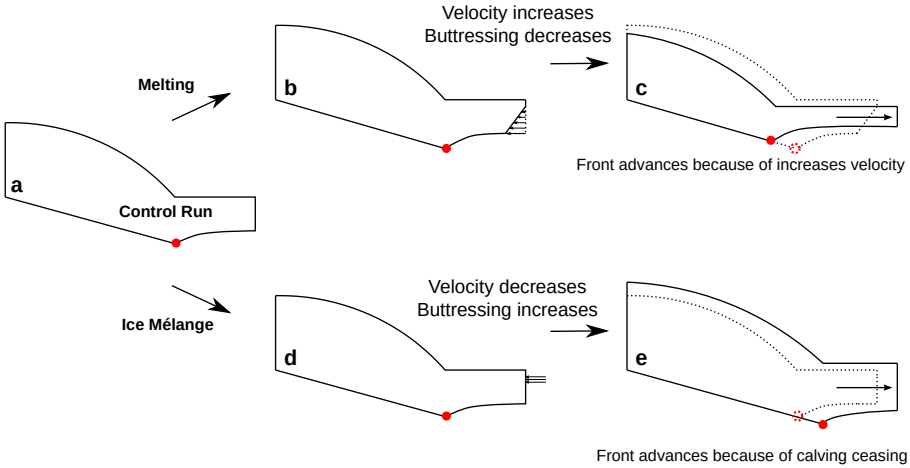

Figure 12. Sketch of the process suggested for glacier equilibrium destabilization. **(a)** Control run disturbed by **(b)** increased melting and **(c)** the resulting stable geometry. **(d)** Ice mélange perturbation and **(e)** resulting stable geometry.

TCD
9, 183–221, 2015